

Southern Ocean ventilation inferred from seasonal cycles of atmospheric N₂O and O₂/N₂ at Cape Grim, Tasmania

By C. D. NEVISON^{1*}, R. F. KEELING², R. F. WEISS², B. N. POPP³, X. JIN⁴, P. J. FRASER⁵, L. W. PORTER⁶ and P. G. HESS¹, ¹National Center for Atmospheric Research, Boulder, CO 80307-3000 USA; ² Scripps Institution of Oceanography, La Jolla, CA 92093-0244 USA; ³ University of Hawaii Honolulu, HI 96822 USA; ⁴ University of California, Los Angeles, CA 90095-4996 USA; ⁵ Commonwealth Scientific and Industrial Research Organization, Atmospheric Research Division, Aspendale, Victoria, Australia; ⁶ Cape Grim Baseline Air Pollution Station, Bureau of Meteorology, Smithton, Tasmania, Australia

(Manuscript received 10 May 2004; in final form 25 November 2004)

ABSTRACT

The seasonal cycle of atmospheric N₂O is derived from a 10-yr observational record at Cape Grim, Tasmania (41°S, 145°E). After correcting for thermal and stratospheric influences, the observed atmospheric seasonal cycle is consistent with the seasonal outgassing of microbially produced N₂O from the Southern Ocean, as predicted by an ocean biogeochemistry model coupled to an atmospheric transport model (ATM). The model–observation comparison suggests a Southern Ocean N₂O source of ~0.9 Tg N yr⁻¹ and is the first study to reproduce observed atmospheric seasonal cycles in N₂O using specified surface sources in forward ATM runs. However, these results are sensitive to the thermal and stratospheric corrections applied to the atmospheric N₂O data. The correlation in subsurface waters between apparent oxygen utilization (AOU) and N₂O production (approximated as the concentration in excess of atmospheric equilibrium ΔN₂O) is exploited to infer the atmospheric seasonal cycle in O₂/N₂ due to ventilation of O₂-depleted subsurface waters. Subtracting this cycle from the observed, thermally corrected seasonal cycle in atmospheric O₂/N₂ allows the residual O₂/N₂ signal from surface net community production to be inferred. Because N₂O is only produced in subsurface ocean waters, where it is correlated to O₂ consumption, atmospheric N₂O observations provide a methodology for distinguishing the surface production and subsurface ventilation signals in atmospheric O₂/N₂, which have previously been inseparable.

1. Introduction

Nitrous oxide (N₂O) is an important atmospheric greenhouse gas with a global warming potential 300 times greater than CO₂ on a per mole basis (Prather et al., 2001). N₂O is destroyed in the stratosphere by photolysis and oxidation and thereby provides the principal source of stratospheric NO_x, an important regulator of stratospheric ozone (Crutzen, 1974; Nevison and Holland, 1997). N₂O is produced by microbial nitrification and denitrification in a wide variety of terrestrial and aquatic ecosystems, whose relative importance is not yet fully quantified or understood (Bouwman et al., 1995). N₂O has been increasing in the atmosphere for the past 100 yr (Weiss, 1981; Machida et al., 1995; Hall et al., 2002). The recent rate of increase suggests a total source that now outpaces the natural stratospheric

sink by ~30%. The increased source is attributed mainly to enhanced microbial production associated with human agriculture (Nevison and Holland, 1997; Mosier et al., 1998; Kroeze et al., 1999). Enhanced N₂O production occurs in agricultural and other perturbed soils as well as in estuaries and coastal areas receiving anthropogenic N runoff (Bange et al., 1996; Seitzinger and Kroeze, 1998; Naqvi et al., 2000; de Bie et al., 2002). In the future, enhanced N₂O production may also occur in oceanic ecosystems, including Southern Ocean regions that potentially may be fertilized with iron (Law and Ling, 2001; Jin and Gruber, 2003).

Recent studies suggest a contradiction in the current N₂O budget for the Southern Ocean. Air–sea flux calculations based on an annual climatology of observed surface N₂O data suggest that the Southern Ocean (defined as all latitudes south of 30°S) emits about one-third of the total oceanic N₂O source (Nevison et al., 1995; Suntharalingam and Sarmiento, 2000). In contrast, estimates of N₂O production based on subsurface data suggest

*Corresponding author.
e-mail: nevison@ucar.edu

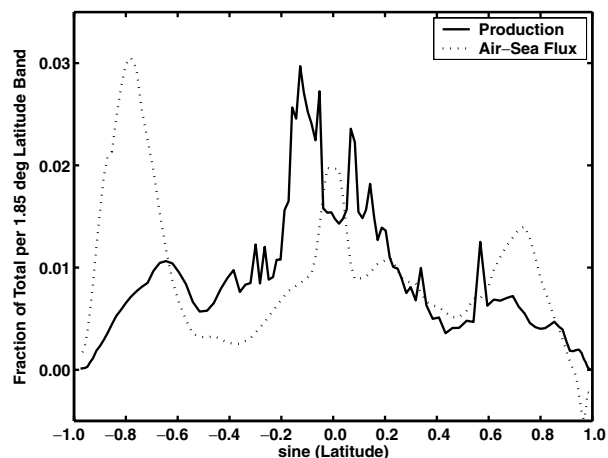


Fig. 1. Dotted line is fraction of total oceanic N_2O source from per latitude band air-sea flux calculations using annual mean ΔpN_2O and monthly varying air-sea transfer coefficients (Nevison et al., 1995, 2004b). Solid line is estimate of N_2O production based on subsurface N_2O data and O_2 consumption predicted by an ocean carbon model (Nevison et al., 2003). The air-sea flux calculation predicts a larger fraction of the N_2O source from the Southern Ocean than the production calculation.

that only $\sim 10\%$ of N_2O is produced at those latitudes (Fig. 1) (Nevison et al., 2003). Notably, the production estimate does not account for N_2O consumption by denitrifying bacteria in low-latitude O_2 -deficient regions (Cohen and Gordon, 1978; Naqvi et al., 1998), nor does it consider that some N_2O produced at low latitudes may ventilate in the Southern Ocean. However, these neglected factors may not be sufficient to resolve the apparent discrepancy.

The record of atmospheric N_2O measured at the Cape Grim, Tasmania ($41^\circ S$, $145^\circ E$) monitoring station can provide additional information about the Southern Ocean N_2O source. The Cape Grim measurements have reached a level of precision sufficient to resolve small but distinct seasonal cycles in N_2O , a long-lived, well-mixed trace gas, which are superimposed upon the more dramatic secular atmospheric increase (Fig. 2). While the latter can be confidently ascribed to global anthropogenically enhanced N_2O sources, the causes of the seasonal cycles have not yet been identified or examined in detail.

Atmospheric transport models (ATMs) provide a potentially important tool for evaluating N_2O sources, through comparison of predicted and observed atmospheric distributions and seasonal cycles. However, past evaluations of N_2O sources in ATMs have revealed poor matches between models and tropospheric observations. Models generally have predicted significant seasonality, whereas observed seasonal cycles were either too small to be detected with past instrumental precision or, in cases where seasonality could be detected, were out of phase with model predictions (Taylor, 1992; Bouwman and Taylor, 1996). In the latter case, the neglected influence of the backflux of N_2O -depleted air from

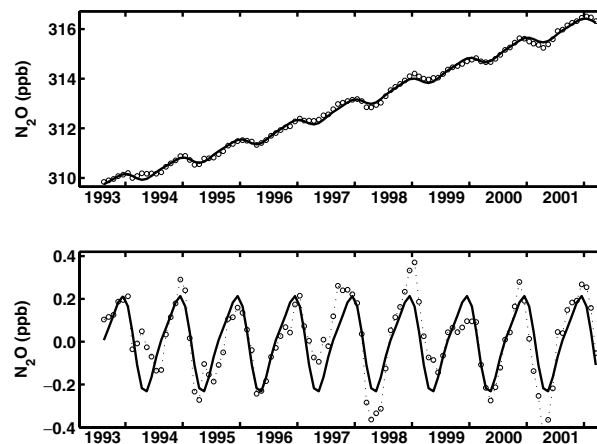


Fig. 2. (a) Time series of AGAGE atmospheric N_2O at Cape Grim, Tasmania ($41^\circ S$, $145^\circ E$). Circles are observed monthly means and the solid line is best fit to the decadal record. (b) Same as (a) after subtracting the polynomial component of the fit to remove the secular trend.

the stratosphere may have contributed to the poor agreement between models and observations (Levin et al., 2002; Liao et al., 2004). Recently, a methodology has been proposed to correct for the stratospheric influence using atmospheric chlorofluorocarbon (CFC) data (Nevison et al., 2004a).

The study presented here is motivated by the need to better understand the Southern Ocean source of the important greenhouse gas N_2O . We approach this question through analysis of atmospheric seasonal cycles observed at Cape Grim and through comparison of the observed cycles with ATM results. Our study differs from previous ATM studies in that, for the first time, we account explicitly for stratospheric influences on observed N_2O seasonal cycles. In addition, whereas previous ATM studies have emphasized seasonal soil emissions and their influence at Northern Hemisphere atmospheric N_2O monitoring stations, we focus on a Southern Hemisphere station surrounded predominantly by oceanic sources. A second aim of our study, described below, is to develop N_2O as a biogeochemical tracer that can provide information about complementary oxygen and carbon cycle processes.

1.1. Biogeochemical links between N_2O and O_2

The well-known anticorrelation between N_2O and oxygen (O_2) in ocean depth profiles (Yoshinari, 1976; Cohen and Gordon, 1978; Butler et al., 1989) is thought to result from the production of N_2O by microbial nitrification in conjunction with O_2 consumption during the oxidation and remineralization of organic matter. The depth profile anticorrelation between N_2O and O_2 is reflected in cross-plot correlations between ΔN_2O and apparent oxygen utilization (AOU). ΔN_2O , the level above atmospheric equilibrium, and $AOU(O_{2,sat} - O_{2,obs})$ provide a measure of the

amount of N_2O produced and O_2 consumed in a water parcel since its last contact with the atmosphere, assuming that outcropping waters are in atmospheric equilibrium.

An important difference between N_2O and O_2 is that N_2O is only produced at depth and is not directly affected by primary production in surface waters, due to the light inhibition of microbial nitrification (Horrigan et al., 1981; Ward, 1986). Therefore, the biological air–sea flux of N_2O reflects purely the ventilation of subsurface water. In contrast, the biological air–sea flux O_2 reflects both ventilation of O_2 -depleted deep water and photosynthetic production of O_2 in surface water. These two processes create competing changes in the surface O_2 saturation anomaly, which complicates the estimate of biological production. In the tropics, for example, the strong influx of O_2 into the ocean due to Equatorial upwelling entirely overwhelms the efflux associated with primary production (Najjar and Keeling, 2000). In the Southern Ocean, the seasonal O_2 signal also reflects the competing and possibly cancelling processes of surface O_2 production and subsurface ventilation. The difficulty in separating these two signals contributes to uncertainty in estimating oceanic biological production from atmospheric O_2/N_2 data (Keeling et al., 1993; Bender et al., 1996; Balkanski et al., 1999; Najjar and Keeling, 2000; Garcia and Keeling, 2001).

Recent evidence from the coast of northern California shows that the $\Delta N_2O/AOU$ correlation in subsurface waters is mirrored by opposing changes in atmospheric N_2O and O_2/N_2 during coastal upwelling events (Lueker et al., 2003). Subsurface waters are rapidly ventilated to the atmosphere during these events, causing a discernible pulse in atmospheric N_2O and a drawdown of atmospheric O_2/N_2 in a molar ratio consistent with the $\Delta N_2O/AOU$ ratio observed in subsurface waters. Like coastal upwelling areas, the Southern Ocean is a region where subsurface waters are ventilated to the atmosphere, particularly in the latitude belt between $35^\circ S$ and $60^\circ S$ that surrounds Cape Grim (Dutay et al., 2002; Takahashi et al., 2002). Atmospheric N_2O measurements at Cape Grim therefore may provide insight into seasonal cycles in atmospheric O_2/N_2 , assuming that the $\Delta N_2O/AOU$ correlation in the Southern Ocean is reflected in atmospheric observations when subsurface waters are ventilated.

We begin our study with a description of the detrending of the Cape Grim N_2O data to infer seasonal cycles, and the removal of thermal and stratospheric influences to isolate the Southern Ocean biological ventilation flux. Next, we compare the atmospheric data with the results of ATM runs with prescribed surface N_2O sources, including output from an ocean biogeochemistry model. Lastly, we use the N_2O biological ventilation flux to partition the observed seasonal cycle in atmospheric O_2/N_2 at Cape Grim into a ventilation flux and a surface production flux. We compare the latter with the seasonal cycle in primary production inferred from satellite chlorophyll data.

2. Atmospheric data analysis at Cape Grim

2.1. AGAGE N_2O and chlorofluorocarbons

Atmospheric N_2O and a variety of CFCs are measured every 40 min by *in situ* gas chromatography at Cape Grim, Tasmania ($41^\circ S$, $145^\circ E$) as part of the Advanced Global Atmospheric Gases Experiment (AGAGE) program (Prinn et al., 2000). Monthly means of these AGAGE data with pollution episodes removed are available online from the Carbon Dioxide Information Analysis Center (CDIAC) (<http://cdiac.ornl.gov>). Since 1993, N_2O has been measured with a precision of about 0.03% (0.1 ppb) for a single measurement, and each monthly mean represents on the order of 10^3 individual measurements. The results are reported on the SIO-1998 calibration scale.

To derive seasonal cycles for the AGAGE data, the monthly means from the 10-yr data set were fitted to a function consisting of a third-order polynomial plus the first four harmonics of the annual cycle. The optimal fit was determined by least-squares regression. The polynomial component was subtracted to remove the secular trend. The remaining harmonic component reveals a small seasonal cycle with a December maximum and a peak-to-trough amplitude of 0.45 ppb (or $\sim 0.14\%$ of the mean mixing ratio of ~ 315 ppb).

In subsequent figures, we show the least-squares best harmonic fit to the 10-yr data set, although we note that the data display significant interannual variability (Fig. 2). The peak-to-trough amplitude of the detrended N_2O residual often deviates by $\sim 20\%$ in any given year from the amplitude of the mean decadal harmonic fit, and in some years can deviate by as much as 60% (Fig. 2b). However, the phasing of the seasonal cycle is consistent from year to year, with a December maximum and an April–May minimum.

We assume that the observed seasonal cycle represents the sum of the following influences:

$$N_2O_{\text{obs}} = N_2O_{\text{stratos}} + N_2O_{\text{vent}} + N_2O_{\text{therm}} + N_2O_{\text{land}}. \quad (1)$$

Among the terms on the right-hand side of eq. (1), we assume that N_2O_{land} is negligible (see discussion of ATM results). The remaining three terms are discussed individually below.

2.2. Thermal cycle: N_2O_{therm}

Both N_2O and O_2 have thermal fluxes associated with their changing solubility in warming and cooling surface waters. These thermal fluxes are significant relative to the biological fluxes over a seasonal cycle (Keeling et al., 1998; Najjar and Keeling, 2000). Argon (Ar), a noble gas that comprises 1% of the Earth's atmosphere, also undergoes seasonal thermal in- and outgassing, but is inert with respect to biological activity. The seasonal cycle in atmospheric Ar is measured as $\delta(\text{Ar}/N_2)$, the change in the Ar/ N_2 ratio relative to a standard. The Ar/ N_2 seasonal cycle at Cape Grim has been modelled, using prescribed

climatological ECMWF air–sea heat fluxes and the TM2 atmospheric transport model, and validated against recent observations (Battle et al., 2003; Keeling et al., 2004). Because the validation exercise suggests that the phasing of the model seasonal cycle is too early relative to observations, due to the idealized assumption of instantaneous air–sea transfer of thermal disequilibrium signals (Battle et al., 2003), we have shifted the model $\delta(\text{Ar}/\text{N}_2)$ results forward by 1 month in the calculations below.

The seasonal cycle in atmospheric Ar/N_2 provides a means to correct biologically active gases like N_2O and O_2 for thermal effects, and thus to isolate biological signals. We calculate the change in atmospheric N_2O due to thermal effects as

$$\text{N}_2\text{O}_{\text{therm}} = 10^{-6} \frac{S_{\text{T},\text{N}_2\text{O}} - S_{\text{T},\text{N}_2}}{S_{\text{T},\text{Ar}} - S_{\text{T},\text{N}_2}} \delta(\text{Ar}/\text{N}_2) X_{\text{N}_2\text{O}}, \quad (2)$$

where $\text{N}_2\text{O}_{\text{therm}}$ is the monthly change from the annual mean in ppb, S_{T} is the thermal derivative of the solubility coefficient (expressed in moles of gas per litre of solution per atmosphere of pure gas per degree Celsius), $\delta(\text{Ar}/\text{N}_2)$ is the modelled monthly change in atmospheric Ar/N_2 relative to the annual mean in per meg, 10^{-6} is a conversion factor from per meg units and $X_{\text{N}_2\text{O}}$ is the average N_2O mixing ratio in ppb. The S_{T} terms are needed to account for thermal fluxes of N_2 that contribute to observed variations in the Ar/N_2 ratio (Keeling et al., 1993). The solubility derivatives are slightly sensitive to the temperature at which they are evaluated. We use a typical annual mean mid-latitude Southern Ocean sea surface temperature of 8°C in our calculations. The resulting thermal cycle of atmospheric N_2O is comparable in amplitude to the observed seasonal cycle, but is 3 months out of phase, with a maximum in February–March (late summer) (Fig. 3). The residual $\text{N}_2\text{O}_{\text{obs}} - \text{N}_2\text{O}_{\text{therm}}$ cycle has a peak to trough amplitude of 0.72 ppb, with a maximum in November (cyan curve in Fig. 3). This residual represents the inferred biological ventilation signal in N_2O prior to making the stratospheric correction discussed below.

The observed Ar/N_2 seasonal cycle at Cape Grim (used to validate the ECMWF-TM2 model) has an amplitude uncertainty of $\pm 30\%$ and a phase uncertainty of 1–2 months (Battle et al., 2003). These uncertainties carry over to $\text{N}_2\text{O}_{\text{therm}}$ and in turn affect the $\text{N}_2\text{O}_{\text{obs}} - \text{N}_2\text{O}_{\text{therm}}$ residual. Sensitivity tests show that the residual is only moderately sensitive to the amplitude uncertainty; a 30% increase in $\text{N}_2\text{O}_{\text{therm}}$ leads to a 15% increase in the amplitude of the $\text{N}_2\text{O}_{\text{obs}} - \text{N}_2\text{O}_{\text{therm}}$ residual, with little effect on its phasing. The residual is somewhat more sensitive to the phasing of $\text{N}_2\text{O}_{\text{therm}}$. When, for example, the Ar/N_2 seasonal cycle from the ECMWF-TM2 model is not shifted forward 1 month, $\text{N}_2\text{O}_{\text{therm}}$ overlaps better with $\text{N}_2\text{O}_{\text{obs}}$. The resulting $\text{N}_2\text{O}_{\text{obs}} - \text{N}_2\text{O}_{\text{therm}}$ residual cycle is 20% smaller in amplitude and peaks 1 month earlier, in October rather than November. In the future, as more Ar/N_2 data become available, it should be possible to reduce the uncertainties in $\text{N}_2\text{O}_{\text{therm}}$ by deriving the Ar/N_2 seasonal cycle directly from a harmonic fit to a multiyear observational record.

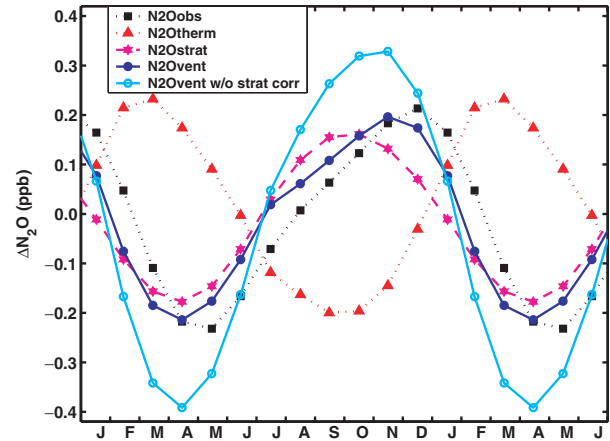


Fig. 3. Seasonal cycle in atmospheric N_2O at Cape Grim, as described by eq. (1) in the text. Black squares are $\text{N}_2\text{O}_{\text{obs}}$, red triangles are $\text{N}_2\text{O}_{\text{therm}}$, $\text{N}_2\text{O}_{\text{strat}}$ (magenta stars) is derived from the F12 seasonal cycle scaled by a $0.72 \text{ N}_2\text{O}/\text{F12}$ scaling factor. $\text{N}_2\text{O}_{\text{land}}$ at Cape Grim is assumed to be negligible based on ATM results. The biological ventilation cycle $\text{N}_2\text{O}_{\text{vent}}$ (solid blue circles) is calculated as the residual of $\text{N}_2\text{O}_{\text{obs}} - \text{N}_2\text{O}_{\text{therm}} - \text{N}_2\text{O}_{\text{strat}}$. Also shown is $\text{N}_2\text{O}_{\text{vent}}$ calculated without the stratospheric correction as $\text{N}_2\text{O}_{\text{obs}} - \text{N}_2\text{O}_{\text{therm}}$ (open cyan circles).

2.3. Stratospheric influence: $\text{N}_2\text{O}_{\text{stratos}}$

Recent work has shown that N_2O , CFC11 and CFC12 have similar tropospheric seasonal cycles at Cape Grim, with well-correlated April–May minima (Nevison et al., 2004a). The correlated minima suggest a common driving mechanism, which might involve the backflux of N_2O and CFC-depleted air from the stratosphere. The N_2O maximum at Cape Grim is notably offset from that of the CFCs, which suggests additional influences from regional N_2O sources. Like N_2O , CFCs are photochemically destroyed in the stratosphere. In contrast to N_2O , however, CFCs are entirely manmade gases with well-known surface sources that largely ceased in 1996. A reasonable first approach to correcting tropospheric N_2O seasonal cycles for stratospheric influences is to subtract the observed tropospheric CFC seasonal cycle (using either CFC11 or CFC12) multiplied by $\text{N}_2\text{O}_{\text{stratos}} \cdot \text{CFC}_{\text{stratos}}$ scaling factors that reflect the relative efficiency of stratospheric removal of the two species (Nevison et al., 2004a).

We calculate CFC seasonal cycles at Cape Grim in a similar manner to N_2O . Observed AGAGE monthly means are fit to a polynomial + harmonic function and detrended by subtracting the polynomial component. The remaining harmonic component, i.e. the observed seasonal cycle, is assumed to reflect the following influences,

$$\text{CFC}_{\text{obs}} = \text{CFC}_{\text{stratos}} + \text{CFC}_{\text{therm}}. \quad (3)$$

CFC_{obs} is corrected for thermal effects using an equation analogous to (2) with the appropriate CFC substituted for N_2O . As

for N_2O , the calculated CFC thermal cycles are out of phase with the observed seasonal cycles. However, in contrast to the large thermal cycle of the more soluble N_2O , the CFC11 thermal cycle is only $\sim 30\%$ of the observed CFC11 amplitude and the CFC12 thermal cycle is only $\sim 15\%$ of the observed CFC12 amplitude.

We derive $N_2O_{\text{stratos}}:CFC_{\text{stratos}}$ scaling factors from observed near-tropopause data measured on a series of ER2 high-altitude aircraft flights from Christchurch, New Zealand ($44^\circ S, 172^\circ E$) in 1994 (Volk et al., 1997). In accordance with stratospheric tracer correlation theory (Plumb and Ko, 1992), the scaling factors are assumed to be the correlation slopes of cross-plots of N_2O versus CFC12 and N_2O versus CFC11, where the slopes $dN_2O/dCFC$ are normalized by the ratio of absolute tropospheric mixing ratios CFC/N_2O . The normalized slopes are 0.72 for $N_2O_{\text{stratos}}:CFC12_{\text{stratos}}$ and 0.38 $N_2O_{\text{stratos}}:CFC11_{\text{stratos}}$, with $\sim 10\%$ uncertainty (Volk et al., 1997, Tables 1–3). The resulting CFC12-based stratospheric correction, N_2O_{stratos} , is 0.34 ppb in amplitude (about 75% of the observed N_2O seasonal cycle), but with a September–October maximum, 2–3 months earlier than the observed seasonal maximum (Fig. 3). The CFC11-based stratospheric N_2O correction (not shown) is similar in phasing, but larger (0.43 ppb) in amplitude. The difference between the CFC11- and CFC12-derived stratospheric terms suggests that the uncertainty in N_2O_{stratos} is at least 25–30%.

An additional caveat on our estimate of N_2O_{stratos} is that, despite circumstantial evidence for a stratospheric influence, we lack solid proof, especially at Southern mid-latitudes (Levin et al., 2002; Nevison et al., 2004a). Furthermore, we cannot rule out additional tropospheric dynamical influences on N_2O seasonal cycles, for example due to interhemispheric mixing. However, our approach to correcting N_2O data based on observed CFC cycles can still be justified based on the more general theory of Plumb and McConalogue (1988), which argues that long-lived trace constituents far from their sources exhibit “universal behaviour”, or simply related variability. According to this theory, we can rewrite eq. (1) as,

$$\begin{aligned} N_2O_{\text{obs}} &= N_2O_{\text{remote}} + N_2O_{\text{regional}} \\ &= N_2O_{\text{remote}} + N_2O_{\text{vent}} + N_2O_{\text{therm}} + N_2O_{\text{land}} \end{aligned} \quad (1')$$

where N_2O_{remote} represents the seasonal cycle due to remote influences, which include but are not necessarily limited to the stratosphere. Since CFCs have few sources near the surface at Cape Grim, we can assume that their observed seasonal cycles (after the small correction for regional thermal influences) can be related simply to N_2O_{remote} through a scaling factor. The observed correlation slope between N_2O and CFCs at a location far from sources of N_2O , i.e. near the tropopause, is still arguably an appropriate $N_2O_{\text{remote}}:CFC_{\text{remote}}$ scaling factor, although with the caveat that the theory of relationships between long-lived tracers has not been well explored observationally in the troposphere (Plumb and McConalogue, 1988).

2.4. Inferred biological ventilation signal: N_2O_{vent}

After subtracting the thermal and stratospheric (or remote) corrections from the observed atmospheric N_2O at Cape Grim, we infer as a residual the seasonal change in atmospheric N_2O due to ventilation of microbially enriched subsurface waters from the Southern Ocean (N_2O_{vent} in eq. (1), Fig. 3). The inferred ventilation cycle is maximum in October–November, with a peak-to-trough amplitude of 0.31 or 0.41 ppb, using the CFC11 and CFC12 stratospheric corrections, respectively. Without the stratospheric correction term, the ventilation cycle is similar in phase but considerably larger, with a peak-to-trough amplitude of 0.72 ppb. The uncertainties discussed above in N_2O_{therm} also carry over to N_2O_{vent} . The N_2O_{therm} phasing uncertainties in particular lead to uncertainties up to 40% in the amplitude of N_2O_{vent} . Collectively, the uncertainties in N_2O_{stratos} and N_2O_{therm} create an uncertainty of at least $\pm 50\%$ in the amplitude and ± 1 month in the phasing of the residual biological ventilation signal N_2O_{vent} .

3. Atmospheric transport model study

In this section, the inferred thermal and biological ventilation signals in atmospheric N_2O are evaluated in forward runs of an atmospheric transport model using prescribed Southern Ocean N_2O fluxes.

3.1. MOZART

MOZART-2 (Model of Ozone and Related Chemical Tracers, version 2) is a global chemical transport model designed to simulate the distribution of tropospheric ozone and its precursors (Horowitz et al., 2003). The model resolution is T42 ($2.8^\circ \times 2.8^\circ$) with 34 hybrid vertical levels extending up to 4 mb (~ 40 km). For this study, the model was driven by 1983–1987 meteorological inputs from the National Center for Environmental Prediction (NCEP) reanalysis. After a model run of 3 yr plus 1 day, seasonal cycles were derived from the Year 3 results by subtracting the linear trend in atmospheric N_2O between 1 January of Year 3 and 1 January of Year 4. Due to its limited stratosphere, MOZART cannot fully reproduce stratospheric chemistry and its influence on tropospheric seasonal cycles. The model was therefore run in transport mode only, with all atmospheric chemistry turned off. As a result, the seasonal cycles should purely reflect the influences of prescribed monthly mean surface sources.

3.2. Prescribed surface fluxes

Various surface sources of N_2O were run as separate tracers. Monthly mean soil N_2O emissions were obtained from the CASA terrestrial biogeochemistry model (Potter et al., 1996). Annual mean anthropogenic emissions were obtained from the Global Emissions Inventory Activity (GEIA) database

(Bouwman et al., 1995). Monthly ocean thermal fluxes were estimated as QS_T/C_p , where Q is monthly mean ocean heat flux from a $1^\circ \times 1^\circ$ gridded database (Grist and Josey, 2003), S_T is the temperature derivative of the N_2O solubility coefficient (Weiss and Price, 1980) and C_p is the assumed specific heat of sea water of $3993 \text{ J kg}^{-1} \text{ K}^{-1}$ (eq. (3) in Najjar and Keeling 2000). Two different ocean biological sources were tested in MOZART, as described below. By treating the sources as separate tracers, the model atmospheric N_2O seasonal cycles at Cape Grim can be decomposed into individual contributions from specific sources.

The first oceanic N_2O source was obtained from the air–sea flux calculation of Nevison et al. (1995, 2004b), in which a global annual composite $0.5^\circ \times 0.5^\circ$ map of ΔpN_2O was gridded and extrapolated from more than 100 000 measurements of the surface N_2O saturation anomaly. The ΔpN_2O data were collected between 1977 and 1996 on expeditions that spanned all world oceans. The air–sea flux was calculated as,

$$F_{\text{vent1}} = kS\Delta pN_2O_{\text{annual}} \quad (4)$$

where F_{vent1} is the flux in $\text{mol m}^{-2} \text{ month}^{-1}$, $\Delta pN_2O_{\text{annual}}$ is the surface anomaly in atm, S is the solubility coefficient of Weiss and Price (1980), calculated using the monthly mean global sea surface temperature climatology of Reynolds et al. (2002), and k is the air–sea transfer velocity calculated from the formula of Wanninkhof (1992). Monthly mean wind speed inputs to k were obtained from a $0.5^\circ \times 0.5^\circ$ blend of NCEP reanalysis products and satellite data from the NASA Quick Scatterometer (Milliff and Morzel, 2001). Since ΔpN_2O is assumed constant over the year, the seasonality in the air–sea flux calculations is driven only by the temporal variations in wind speed and sea surface temperature (Fig. 4). After interpolating to the MOZART T42 grid, the total ocean source F_{vent1} is $3.9 \text{ Tg N}_2\text{O-N yr}^{-1}$, with $1.5 \text{ Tg N}_2\text{O-N yr}^{-1}$, more than a third of the total, emitted between 30° and 90°S (Fig. 1). An analysis of the ΔpN_2O dataset (see discussion below) suggests that, although we have lumped the F_{vent1} air–sea fluxes into the category of “biological ventilation”, the global composite $\Delta pN_2O_{\text{annual}}$ map actually reflects a mix of biological and thermal influences.

The second ocean source F_{vent2} was obtained from a three-dimensional ocean physical–biogeochemical model, in which N_2O production is parametrized as a function of O_2 consumption (Jin and Gruber, 2003). The parameterization is based on the well-known correlation between ΔN_2O and AOU in ocean depth profiles. F_{vent2} has a strong peak in August–September (Fig. 4), which is caused primarily by the increase in vertical transport of N_2O into surface waters associated with the wintertime deepening of the mixed layer. The seasonal changes in mixed layer depth predicted by the ocean model compare well with observations. The model calculates its own thermal N_2O flux, which was also tested in MOZART. The total F_{vent2} ocean source is $3.7 \text{ Tg N}_2\text{O-N yr}^{-1}$, with $0.9 \text{ Tg N}_2\text{O-N yr}^{-1}$ emitted between 30° and 90°S .

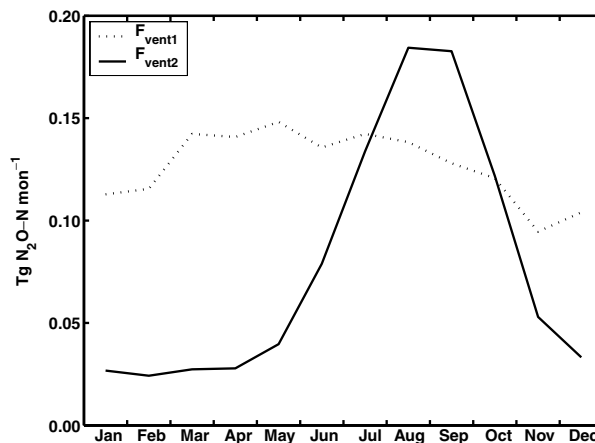


Fig. 4. Two monthly mean oceanic N_2O sources tested in MOZART. F_{vent1} (dotted line) is calculated from an annual composite map of observed ΔpN_2O multiplied by seasonal air–sea transfer coefficients (Nevison et al., 1995, 2004b), F_{vent2} (solid line) is calculated by the ocean biogeochemistry model of Jin and Gruber (2003).

3.3. ATM results

We compared the seasonal cycles at Cape Grim predicted by MOZART, run with F_{vent1} and F_{vent2} , with the inferred biological ventilation cycle at Cape Grim, N_2O_{vent} , described above. As can be predicted from its relative lack of seasonality (Fig. 4), F_{vent1} yields no coherent seasonal cycle in atmospheric N_2O and thus matches poorly with observations. In contrast, the ocean biogeochemistry model (F_{vent2}) yields a seasonal cycle of similar amplitude and phasing to the inferred ventilation cycle (Fig. 5).

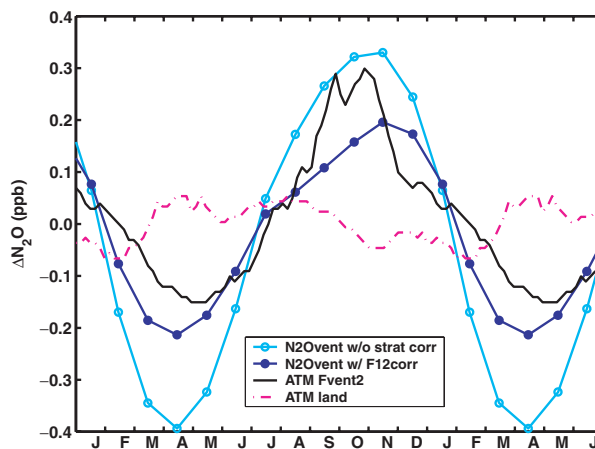


Fig. 5. Comparison of MOZART ATM results to the inferred ventilation cycle in atmospheric N_2O at Cape Grim. The black solid line is ATM run with F_{vent2} . N_2O_{vent} inferred from AGAGE atmospheric data at Cape Grim as described in Fig. 3 is shown for comparison. Open cyan circles are with only the thermal correction to the observed data. Solid blue circles are with both the thermal and stratospheric corrections. Also shown are ATM results with the CASA soil source (dot-dashed magenta line).

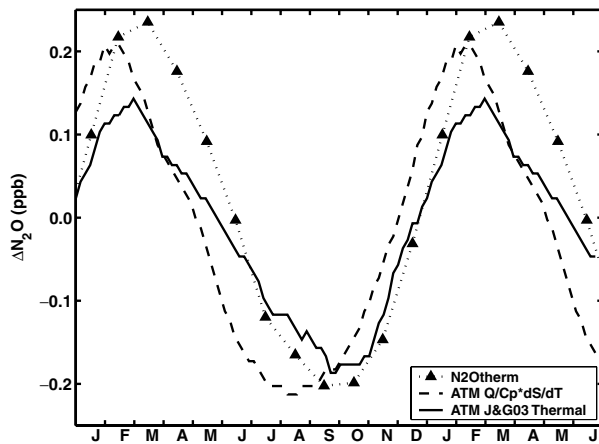


Fig. 6. MOZART ATM results compared with the estimated thermal cycle in atmospheric N_2O at Cape Grim. The dashed line is the ATM run with the heat-flux-based thermal N_2O flux QS_T/C_p ; the solid line is the ATM run with the thermal flux from the ocean biogeochemistry model of Jin and Gruber (2003). Model results are compared with N_2O_{therm} , as inferred from Ar/N_2 scaled to N_2O by eq. (2) (triangles).

The F_{vent2} results suggest that our inferred atmospheric spring maximum in N_2O_{vent} is consistent with the cumulative effect of oceanic ventilation that peaks in late winter (Fig. 4).

The ATM study provides support for the thermal correction N_2O_{therm} in eq. (1). MOZART runs with both the heat-flux-based (QS_T/C_p) and ocean biogeochemistry model thermal N_2O fluxes agree fairly well with the atmospheric N_2O cycle at Cape Grim derived from Ar/N_2 data, although the MOZART heat-flux-based maximum is ~ 1 month early (Fig. 6). As discussed in Section 2.2, this early maximum reflects the fact that the QS_T/C_p equation neglects delays in the adjustment of the dissolved N_2O concentration to its new thermal equilibrium as ocean waters warm or cool.

The ATM study offers justification for neglecting N_2O_{land} in eq. (1). MOZART runs show that the CASA soil N_2O source produces some seasonal variability but no coherent seasonal cycle in atmospheric N_2O at the latitude of Cape Grim (Fig. 5). Decomposition of the soil source by region shows that the variability at Cape Grim stems mainly from the southern tropics rather than from local mid-latitude soil sources. The anthropogenic N_2O source is only available at annual resolution and therefore produces no seasonality in atmospheric N_2O . In any case, it is very small around Cape Grim according to the GEIA database.

3.4. Additional evidence of a ventilation signal

The strong seasonality of the N_2O source suggested by the F_{vent2} -ATM results prompted us to partition the observed 100 000-point ΔpN_2O database used to estimate F_{vent1} by month. From the partitioned data set, we calculated the mean ΔpN_2O from 40° – 60° S as a function of month (Fig. 7). Although the data are sparse, the

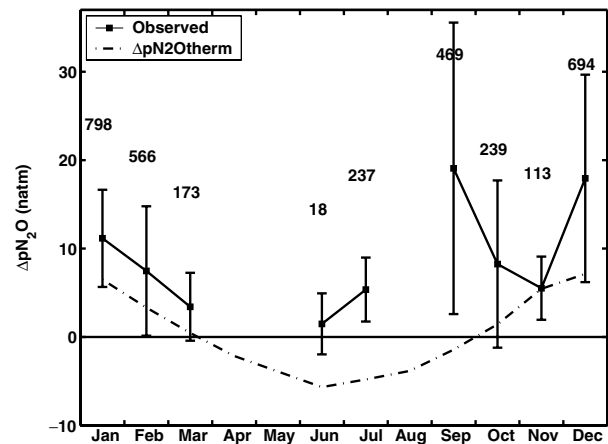


Fig. 7. Monthly mean ΔpN_2O in the 40 – 60° S latitude band (squares), taken from the 100 000 point surface database (Nevison et al., 2004b). Gaps indicate no data. Text annotations reflect the number of data points in each monthly bin. Standard deviations are shown as error bars. For comparison, the dot-dashed line is a simple estimate of the solubility driven increase in ΔpN_2O derived by solving $QS_T/C_p = kS\Delta pN_2O_{therm}$ for ΔpN_2O_{therm} , where Q , S_T , C_p , k and S are estimated as described in the text. Observed seasonal changes in ΔpN_2O appear to be consistent with summertime thermal enhancement and wintertime enhancement due to deep-water ventilation.

results show that the highest values of ΔpN_2O are found in late winter (September) and also in summer (December–January). A simple estimate of the solubility-driven increase in ΔpN_2O due to changing sea surface temperature suggests that the summer maxima can be attributed to thermal effects. In contrast, the late winter highs are more likely to be a biological signal associated with entrainment of N_2O -enriched deep water. Thus, observed seasonal changes in ΔpN_2O appear to be at least qualitatively consistent with the ocean carbon model's prediction of an August–September ventilation maximum.

Isotopic signatures of N_2O in the Sub-Antarctic Zone are also consistent with ventilation of the Southern Ocean. Nitrogen and oxygen isotopic compositions of dissolved N_2O from four stations in the Sub-Antarctic Zone south of Australia (42° S to 54° S along $\sim 142^\circ$ E) are close to isotopic equilibrium with the atmosphere and vary little at depths shallower than 800 m (Table 1). The lack of isotopic variation with depth is striking compared with low-latitude sites where isotopic compositions of N_2O have been measured. Most oceanic profiles show $\delta^{18}O$ values increasing markedly with depth, reaching values in excess of $+50\%$ versus standard mean ocean water (SMOW) within the upper 1000 m (e.g. Kim and Craig, 1990; Popp et al., 2002; Toyoda et al., 2002). Winter mixing in the Sub-Antarctic Zone typically extends to depths >400 m and results in the formation of Sub-Antarctic Mode Water (Rintoul and Trull, 2001). Seasonal ventilation and the formation of Sub-Antarctic Mode Water best explain the lack of variation in the isotopic compositions of N_2O

Table 1. Summary of $\delta^{15}\text{N}$ and $\delta^{18}\text{O}$ values of N_2O in the atmosphere and in the Sub-Antarctic Zone measured in February–March, 1998 during the SAZ cruise on the R/V *Aurora Australis*. Analytical uncertainty and methods are described in Popp et al. (2002)

Location	Depth range (m)	$\delta^{15}\text{N}$ (‰) vs air	± 1 SD	$\delta^{18}\text{O}$ (‰) vs SMOW	± 1 SD	n
42°S,142°E	0–800	8.2	0.8	44.6	0.8	15
	1000–4000	9.1	0.8	48.8	1.5	5
47°S,142°E	0–800	8.1	1.0	44.2	1.3	25
	1000–3500	8.6	1.2	46.3	2.3	5
51°S,143°E	0–800	8.5	1.5	45.4	1.4	10
	1000–1500	8.9	0.2	47.6	0.5	2
54°S,142°E	0–800	8.5	1.5	45.3	1.4	9
	1000–2825	8.9	0.5	48.6	0.4	5
All stations	Atmospheric	7.3	0.8	43.5	0.5	6

and the fact that the values are close to equilibrium with atmospheric N_2O in the Sub-Antarctic Zone of the Southern Ocean.

3.5. Discussion

At present, the strongest conclusion we can draw from the ATM exercises and our review of observational evidence is that $\Delta p\text{N}_2\text{O}$ cannot be treated as an annual constant in the Southern Ocean. Rather, it is a quantity that varies strongly with season, with enhancements in summer due to thermal effects and larger enhancements in late winter due to entrainment of N_2O -enriched deep water into the mixed layer. Since $\Delta p\text{N}_2\text{O}$ observations have been made predominantly during months of enhancement (Fig. 7), the global annual composite $\Delta p\text{N}_2\text{O}_{\text{annual}}$ of Nevison et al. (1995, 2004b) most likely overestimates the true annual mean surface N_2O anomaly. This overestimate may explain much of the apparent discrepancy in the latitudinal distributions of F_{vent1} versus estimates of N_2O production based on subsurface data (Fig. 1).

Our conclusions about the magnitude of the Southern Ocean source are more tentative, due in part to uncertainty associated with the thermal and stratospheric corrections to atmospheric N_2O data. In addition, our analysis is not well suited to inferring absolute source magnitudes, since we have subtracted absolute mean atmospheric mixing ratios to focus on small residual seasonal cycles. However, we suggest, based on comparison of the ATM F_{vent2} run to the observed ventilation signal $\text{N}_2\text{O}_{\text{vent}}$ (Fig. 5), that the available evidence is consistent with a Southern Ocean N_2O source of $\sim 0.9 \text{ Tg N yr}^{-1}$. Improved understanding of the thermal and stratospheric corrections and comparison of ATM results with atmospheric data across spatial gradients can help place firmer constraints on this source.

4. Atmospheric O_2/N_2 cycle

The seasonal cycle in atmospheric O_2/N_2 data at Cape Grim was derived from the best harmonic + polynomial fit to 10 yr

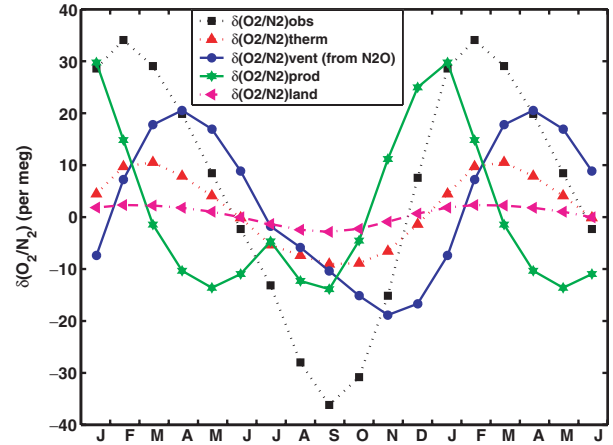


Fig. 8. Seasonal cycle in atmospheric $\delta(\text{O}_2/\text{N}_2)$ at Cape Grim, as described by eq. (6) in the text. Black squares are $\delta(\text{O}_2/\text{N}_2)_{\text{obs}}$. Red triangles are $\delta(\text{O}_2/\text{N}_2)_{\text{therm}}$. Magenta sideways triangles are $\delta(\text{O}_2/\text{N}_2)_{\text{land}}$. The signal due to ventilation of O_2 -depleted deep water $\delta(\text{O}_2/\text{N}_2)_{\text{vent}}$ (blue circles) is inferred from $\text{N}_2\text{O}_{\text{vent}}$ in Fig. 3 (with thermal and stratospheric corrections). The signal due to production of O_2 in the euphotic surface layer $\delta(\text{O}_2/\text{N}_2)_{\text{prod}}$ is inferred as a residual (green stars).

of monthly mean observations using a methodology similar to our treatment of the atmospheric N_2O and CFC data (Keeling and Shertz, 1992; Keeling et al., 1996, 1998). The small secular decline in O_2/N_2 due to fossil fuel combustion was removed by subtracting the polynomial component of the fit. The atmospheric O_2/N_2 ratio, like the Ar/N_2 ratio, is measured in per meg units. The O_2/N_2 seasonal cycle is corrected for thermal effects in a similar manner to N_2O , except that the conversion from per meg units is no longer needed (Fig. 8):

$$\delta(\text{O}_2/\text{N}_2)_{\text{therm}} = \frac{S_{\text{T},\text{O}_2} - S_{\text{T},\text{N}_2}}{S_{\text{T},\text{Ar}} - S_{\text{T},\text{N}_2}} \delta(\text{Ar}/\text{N}_2). \quad (5)$$

As for N_2O , we can decompose the observed seasonal cycle in atmospheric O_2 into the sum of oceanic biological and thermal components and terrestrial components:

$$\delta(\text{O}_2/\text{N}_2)_{\text{obs}} = \delta(\text{O}_2/\text{N}_2)_{\text{vent}} + \delta(\text{O}_2/\text{N}_2)_{\text{prod}} + \delta(\text{O}_2/\text{N}_2)_{\text{therm}} + \delta(\text{O}_2/\text{N}_2)_{\text{land}}. \quad (6)$$

Although some O_2 is photolysed in the stratosphere to maintain a dynamic concentration of ozone (O_3), this O_2 loss is too small to be significant relative to the surface source/sink terms for O_2 . Furthermore, the very long atmospheric lifetime of O_2 suggests that any additional remote influences are negligible relative to regional influences. Hence, we neglect any stratospheric or remote correction term. The land influence can be estimated as $1.1/0.2095 \text{ CO}_2$, where CO_2 is the detrended decadal mean seasonal cycle in atmospheric CO_2 in ppm, 0.2095 is a conversion from ppm to per meg units, and 1.1 is the assumed approximate ratio of $-\text{dO}_2:\text{dCO}_2$ due to terrestrial photosynthesis and respiration (Stephens et al., 1998; Lueker et al., 2003). Using

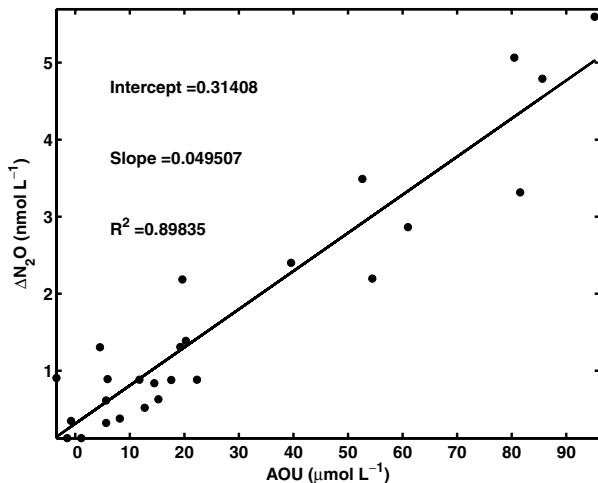


Fig. 9. ΔN_2O versus apparent oxygen utilization (AOU) for data from the Sub-Antarctic Zone (SAZ) Project. Data were collected in February–March, 1998 in the Southern Ocean south of Australia at five stations from 42° – 51° S, $\sim 142^\circ$ E using the methodology described in Popp et al. (2002). The correlation slope for all data between potential density surfaces $\sigma_\theta = 26.5$ – 27.1 is 50 ± 10 nmol N_2O/μ mol AOU.

NOAA CO_2 data (www.cmdl.noaa.gov/ccgg), we find that the land term (magenta curve in Fig. 8) is small at the mainly oceanic Cape Grim station, and tends to reduce $\delta(O_2/N_2)_{obs}$ by 10% or less.

The crux of our analysis rests on using the inferred ventilation cycle in atmospheric N_2O to estimate the corresponding biological ventilation signal in atmospheric O_2/N_2 , i.e. $\delta(O_2/N_2)_{vent}$. Using Sub-Antarctic Zone concentration data (from 42° S to 54° S along $\sim 142^\circ$ E), we estimate a $\Delta N_2O/AOU$ correlation of -50 ± 10 μ mol mol^{-1} for the subsurface waters in the region around Cape Grim (Fig. 9). NOAA data from the eastern Pacific and Atlantic sectors of the Southern Ocean yield a similar $\Delta N_2O/AOU$ correlation slope (Nevison et al., 2003). Assuming the $\Delta N_2O/AOU$ ratio is reflected in atmospheric variations in N_2O and O_2/N_2 when subsurface waters are ventilated, we calculate $\delta(O_2/N_2)_{vent}$ by dividing $\Delta N_2O/AOU$ into N_2O_{vent} and converting to per meg units. The result is the seasonal cycle in atmospheric O_2/N_2 due to ventilation of subsurface waters depleted in O_2 by microbial respiration (Fig. 8). $\delta(O_2/N_2)_{vent}$ reaches its minimum in spring, again, as for N_2O , representing the cumulative effect on the atmosphere of oceanic ventilation that peaks in late winter.

4.1. Surface production signal

In contrast to N_2O , there are two biological components of the O_2/N_2 cycle with respect to air–sea gas exchange. We have estimated the first of these, $\delta(O_2/N_2)_{vent}$, from N_2O data. In addition, we have calculated $\delta(O_2/N_2)_{therm}$ from Ar/N_2 data and calculated $\delta(O_2/N_2)_{land}$ from CO_2 data. As a result, the second

biological component $\delta(O_2/N_2)_{prod}$ is the only remaining term in eq. (6) and can be inferred as a residual. $\delta(O_2/N_2)_{prod}$ represents the component of the seasonal cycle in atmospheric O_2/N_2 due to net community production (NCP) in surface waters. (NCP is the gross production of O_2 by photosynthesizers minus the fraction that is quickly reconsumed by respiration in the mixed layer.) The inferred cycle in $\delta(O_2/N_2)_{prod}$ is maximum in summer, with a springtime rise that overlaps significantly with the minimum in $\delta(O_2/N_2)_{vent}$. The overlap between $\delta(O_2/N_2)_{prod}$ and $\delta(O_2/N_2)_{vent}$ suggests that the competition between these terms should be considered in efforts to estimate oceanic biological production using atmospheric O_2/N_2 variations.

A comparison of our inferred $\delta(O_2/N_2)_{prod}$ cycle with the seasonal cycle in primary production, inferred in a completely independent manner from Sea-viewing Wide Field-of-view Sensor (SeaWiFS) chlorophyll data, reveals a number of similarities (Fig. 10). The SeaWiFS data were converted to $g\ C\ m^{-2}\ day^{-1}$ using the algorithm of Behrenfeld and Falkowski (1997) as described in Moore and Abbott (2000). The comparison of $\delta(O_2/N_2)_{prod}$ and SeaWiFS data must be qualified with several remarks. First, the $\delta(O_2/N_2)_{prod}$ cycle represents the seasonal component of the production signal, after subtracting the annual mean. Thus, the zero crossing in $\delta(O_2/N_2)_{prod}$ does not necessarily reflect a time of zero production. Second, SeaWiFS results reflect total primary production, much of which is quickly respired in the mixed layer with no effect on atmospheric O_2 (Keeling et al., 1993). SeaWiFS production can be converted to NCP using assumed f ratios (NCP/total primary production). However, the estimated f ratios in the mid-latitude Southern Ocean are uncertain, ranging from 0.3–0.57, with largest values likely in spring

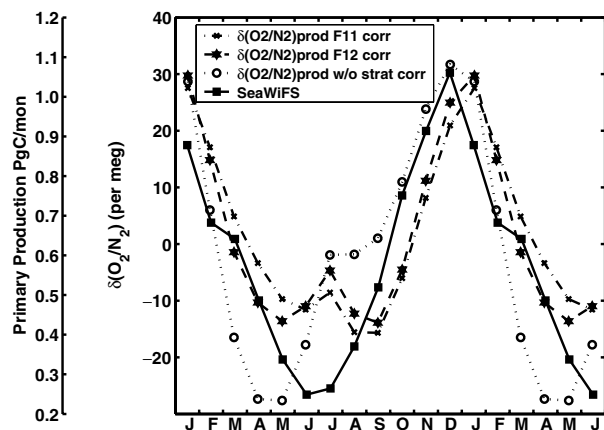


Fig. 10. The component of the seasonal cycle in atmospheric O_2 due to surface production $\delta(O_2/N_2)_{prod}$, calculated without the stratospheric correction to N_2O data (open circles), calculated with the F11-based stratospheric (crosses), and calculated with the F12-based correction (stars). Shown for comparison is monthly primary production integrated from 40° – 60° S derived from SeaWiFS chlorophyll data (Moore and Abbott, 2000) (squares). See text for discussion of caveats associated with this comparison.

(Bender et al., 1996; Balkanski et al., 1999; Moore and Abbott, 2000).

A third and perhaps most important caveat is that the SeaWiFS data reflect surface production directly at the time of measurement, whereas $\delta(\text{O}_2/\text{N}_2)_{\text{prod}}$ reflects the cumulative effect on the atmosphere of air–sea O_2 fluxes associated with NCP. Based on our ATM results with air–sea N_2O fluxes, we predict a delay of 1–2 months between the SeaWiFS maximum and the $\delta(\text{O}_2/\text{N}_2)_{\text{prod}}$ maximum. Consistent with this prediction, the SeaWiFS primary production curve begins rising in August to a maximum in December, whereas the $\delta(\text{O}_2/\text{N}_2)_{\text{prod}}$ cycle begins rising in October to a maximum in January. While these differences could reflect a realistic time delay in the outgassing of O_2 -enriched productive surface waters and the integrated impact on the atmosphere, we must also acknowledge the uncertainties in $\delta(\text{O}_2/\text{N}_2)_{\text{prod}}$ that carry over from the uncertainties in the thermal and, in particular, the stratospheric corrections to the Cape Grim N_2O data. Without the stratospheric correction, the inferred $\delta(\text{O}_2/\text{N}_2)_{\text{prod}}$ cycle begins its seasonal rise around September and is maximum in December. However, the uncorrected cycle displays an obviously erroneous minimum in April–May with an inexplicable steep rise in mid-winter from May to July (Fig. 10). Thus, the decomposition of the O_2/N_2 cycle presented here tends to support a stratospheric or remote influence on the N_2O seasonal cycle.

5. Conclusions

The atmospheric cycles of N_2O and O_2 observed at Cape Grim, Tasmania are consistent with the seasonal ventilation of N_2O -enriched/ O_2 -depleted deep water from the Southern Ocean. The observed atmospheric N_2O cycle appears to be the sum of several terms, all of roughly the same magnitude but different phasing, which include biological ventilation, thermal in- and outgassing, and a stratospheric or remote influence, which as yet is not well understood. The N_2O biological ventilation flux predicted by an ocean carbon model has a strong seasonal maximum in late winter due to entrainment of microbially enriched deep water. The ocean carbon model flux reproduces the phase and amplitude of the inferred ventilation signal in atmospheric N_2O in forward ATM runs, and comparison of ATM results and atmospheric data suggests a Southern Ocean (30° – 90° S) source of about $0.9 \text{ Tg N}_2\text{O-N yr}^{-1}$. However, these conclusions are based on a ventilation signal in atmospheric N_2O that is calculated as the residual of the observed seasonal cycle and two uncertain corrections due to thermal and stratospheric influences.

While more work is needed to better understand and quantify the thermal and stratospheric corrections, the results presented here suggest that atmospheric N_2O data in combination with subsurface $\Delta\text{N}_2\text{O}/\text{AOU}$ ratios can be used to separate atmospheric O_2 signals due to oceanic ventilation and surface production. Our study marks the first observationally based effort to separate these two signals and demonstrates the potential for

using N_2O data to provide insight into the oceanic O_2 cycle. Conversely, the reasonable agreement between the inferred O_2 surface production signal and the seasonal cycle in SeaWiFS primary production provides support for our interpretation of the Cape Grim N_2O data as a signal of Southern Ocean ventilation.

6. Acknowledgments

CDN thanks NSF Grant OCE0096404 and the Biogeosciences Initiative and Atmospheric Chemistry Division of the National Center for Atmospheric Research (NCAR) for their support of her work. NCAR is operated by the University Corporation for Atmospheric Research under the sponsorship of the National Science Foundation. BNP thanks NSF (grants OCE9810640 and OCE0240787) for support of his research on N_2O . We also acknowledge support from the Antarctic CRC SAZ Project and Australian Antarctic Science Grant no 1156 (T. Trull). We thank NASA for their support of the US contributions to AGAGE, David Baker for useful discussions and assistance with the MOZART model, Chris Potter for providing CASA soil model output, and Mark Battle and an anonymous reviewer for helpful comments.

References

- Balkanski, Y., Monfray, P., Battle, M. and Heimann, M. 1999. Ocean primary production derived from satellite data: an evaluation with atmospheric oxygen measurements. *Global Biogeochem. Cycles* **13**, 257–271.
- Bange, H. W., Rapsomanikis, S. and Andreae, M. O. 1996. Nitrous oxide in coastal waters. *Global Biogeochem. Cycles* **10**, 197–207.
- Battle, M., Bender, M., Hendricks, M. B., Ho, D. T., Mika, R. and co-authors 2003. Measurements and models of the atmospheric Ar/ N_2 ratio. *Geophys. Res. Lett.* **30**, 1786, doi:10.1029/2003GL017411.
- Behrenfeld, M. J. and Falkowski, P. G. 1997. Photosynthetic rates derived from satellite-based chlorophyll concentration. *Limnol. Oceanogr.* **42**, 1–20.
- Bender, M., Ellis, T., Tans, P., Francey, R. and Lowe, D. 1996. Variability in the O_2/N_2 ratio of southern hemisphere air, 1991–1994: Implications for the carbon cycle. *Global Biogeochem. Cycles* **10**, 9–21.
- Bouwman, A. F. and Taylor, J. A. 1996. Testing high-resolution nitrous oxide emission estimates against observations using an atmospheric transport model. *Global Biogeochem. Cycles* **10**, 307–318.
- Bouwman, A. F., van der Hoek, K. W. and Olivier, J. G. J. 1995. Testing high-resolution nitrous oxide emission estimates against observations using an atmospheric transport model. *J. Geophys. Res.* **100**, 2785–2800.
- Butler, J. H., Elkins, J. W. and Thompson, T. M. 1989. Tropospheric and dissolved N_2O of the west Pacific and east Indian Oceans during the El Niño Southern Oscillation event of 1987. *J. Geophys. Res.* **94**, 14 865–14 877.
- Cohen, Y. and Gordon, L. I. 1978. Nitrous oxide in the oxygen minimum of the eastern tropical North Pacific: evidence for its consumption during denitrification and possible mechanisms for its production. *Deep-Sea Res.* **25**, 509–524.

- Crutzen, P. J. 1974. Estimates of possible variations in total ozone due to natural causes and human activities. *Ambio* **3**, 201–210.
- de Bie, M. J. M., Middelburg, J. J., Starink, M. and Laanbroek, H. J. 2002. Factors controlling nitrous oxide at the microbial community and estuarine scale. *Mar. Ecol. Prog. Ser.* **240**, 1–9.
- Dutay, J.-C., Bullister, J. L., Doney, S. C., Orr, J. C., Najjar, R. and co-authors 2002. Evaluation of ocean model ventilation with CFC-11: comparison of 13 global models. *Ocean Modelling* **4**, 89–120.
- Garcia, H. E. and Keeling, R. F. 2001. On the global oxygen anomaly and air-sea flux. *J. Geophys. Res.* **106**(C12), 31 155–31 166.
- Grist, J. P. and Josey, S. A. 2003. Inverse analysis adjustment of the SOC air-sea flux climatology using ocean heat transport constraints. *J. Clim.* **16**, 3274–3295.
- Hall, B. D., Butler, J. H., Clarke, A. D., Dutton, G. S., Elkins, J. W. and co-authors 2002. Halocarbons and other atmospheric trace species. In: *CMDL Summary Report 26* Chapter 5 (eds D. B. King, R. C. Schnell, R. M. Rosson and C. Sweet). US Department of Commerce, National Oceanic and Atmospheric Administration, Boulder, CO.
- Horowitz, L. W., Walters, S., Mauzerall, D. L., Emmons, L. K., Rasch, P. J. and co-authors 2003. A global simulation of tropospheric ozone and related tracers: description and evaluation of MOZART, version 2. *J. Geophys. Res.* **108**(D24), 4784, doi:10.1029/2002JD002853.
- Horrigan, S. G., Carlucci, A. F. and Williams, P. M. 1981. Light inhibition of nitrification in sea-surface films. *J. Mar. Res.* **39**, 557–565.
- Jin, X. and Gruber, N. 2003. Offsetting the radiative benefit of ocean iron fertilization by enhancing N₂O emissions. *Geophys. Res. Lett.* **30**(24), 2249.
- Keeling, R. F., Blaine, T., Paplawsky, B., Katz, L., Atwood, C. and co-author 2004. Measurement of changes in atmospheric Ar/N₂ ratio using a rapid-switching, single-capillary mass spectrometer system. *Tellus* **56B**, 322–338.
- Keeling, R. F., Najjar, R. G., Bender, M. L. and Tans, P. P. 1993. What atmospheric oxygen measurements can tell us about the global carbon cycle. *Global Biogeochem. Cycles* **7**(1), 37–67.
- Keeling, R. F., Piper, S. C. and Heimann, M. 1996. Global and hemispheric CO₂ sinks deduced from changes in atmospheric O₂ concentration. *Nature* **381**, 218–221.
- Keeling, R. F. and Shertz, S. R. 1992. Seasonal and interannual variations in atmospheric oxygen and implications for the global carbon cycle. *Nature* **358**, 723–727.
- Keeling, R. F., Stephens, B. B., Najjar, R. G., Doney, S. C., Archer, D. and co-author 1998. Seasonal variations in the atmospheric O₂/N₂ ratio in relation to the kinetics of air-sea gas exchange. *Global Biogeochem. Cycles* **12**(1), 141–163.
- Kim, K. -R. and Craig, H. 1990. Two-isotope characterization of N₂O in the Pacific Ocean and constraints on its origin in deep water. *Nature* **347**, 58–61.
- Kroeze, C., Mosier, A. and Bouwman, L. 1999. Closing the global N₂O budget: a retrospective analysis 1500–1994. *Global Biogeochem. Cycles* **13**, 1–8.
- Law, C. S. and Ling, R. D. 2001. Nitrous oxide flux and response to increased iron availability in the Antarctic Circumpolar Current. *Deep-Sea Res. II* **48**, 2509–2527.
- Levin, I., Ciais, P., Langenfelds, R., Schmidt, M., Ramonet, M. and co-authors 2002. Three years of trace gas observations over the EuroSiberian domain derived from aircraft sampling—a concerted action. *Tellus* **54B**, 696–712.
- Liao, T., Camp, C. D. and Yung, Y. L. 2004. The seasonal cycle of N₂O. *Geophys. Res. Lett.* **31**, 17 108.
- Lueker, T. J., Walker, S. J., Vollmer, M. K., Keeling, R. F., Nevison, C. D. and co-author 2003. Coastal upwelling air-sea fluxes revealed in atmospheric observations of O₂/N₂, CO₂ and N₂O. *Geophys. Res. Lett.* **30**, 1292.
- Machida, T., Nakazawa, T., Tanaka, M., Fufii, Y., Aoki, S. and co-author 1995. Atmospheric methane and nitrous oxide concentrations during the last 250 years. *Geophys. Res. Lett.* **22**, 2921–2924.
- Milliff, R. F. and Morzel, J. 2001. The global distribution of the time average wind stress curl from NSCAT. *J. Atmos. Sci.* **58**, 109.
- Moore, J. K. and Abbott, M. R. 2000. Phytoplankton chlorophyll distributions and primary production in the Southern Ocean. *J. Geophys. Res.* **105**(C12), 28 709–28 722.
- Mosier, A., Kroeze, C., Nevison, C., Oenema, O., Seitzinger, S. and co-author 1998. Closing the global atmospheric N₂O budget: nitrous oxide emissions through the agricultural nitrogen cycle. *Nutrient Cycling Agroecosyst.* **52**, 225–248.
- Najjar, R. G. and Keeling, R. F. 2000. Mean annual cycle of the air-sea oxygen flux: a global view. *Global Biogeochem. Cycles* **14**(2), 573–584.
- Naqvi, S. W. A., Jayakumar, D. A., Narvekar, P. V., Naik, H., Sarma, V. V. S. S. and co-authors 2000. Increased marine production of N₂O due to intensifying anoxia on the Indian continental shelf. *Nature* **408**, 346–349.
- Naqvi, S. W. A., Yoshinari, T., Jayakumar, D. A., Altabet, M. A., Narvekar, P. V. and co-authors 1998. Budgetary and biogeochemical implications of N₂O isotope signatures in the Arabian Sea. *Nature* **394**, 462–464.
- Nevison, C. D. and Holland, E. A. 1997. A reexamination of the impact of anthropogenically fixed nitrogen on atmospheric N₂O and the stratospheric O₃ layer. *J. Geophys. Res.* **102**, 25 519–25 536.
- Nevison, C. D., Butler, J. H. and Elkins, J. W. 2003. Global distribution of N₂O and the Δ N₂O/AOU ratio in the subsurface ocean. *Global Biogeochem. Cycles* **17**(4), 1119.
- Nevison, C. D., Kinnison, D. E. and Weiss, R. F. 2004a. Stratospheric influence on the tropospheric seasonal cycles of nitrous oxide and chlorofluorocarbons. *Geophys. Res. Lett.* **31**(20), L20103, doi:10.1029/2004GL020398.
- Nevison, C. D., Lueker, T. J. and Weiss, R. F. 2004b. Quantifying the nitrous oxide source from coastal upwelling. *Global Biogeochem. Cycles* **18**(1), 1018.
- Nevison, C. D., Weiss, R. F. and Erickson, D. J. 1995. Global oceanic emissions of nitrous oxide. *J. Geophys. Res. Oceans* **100**(C8), 15 809–15 820.
- Plumb, R. A. and Ko, M. K. W. 1992. Interrelationships between mixing ratios of long-lived stratospheric constituents. *J. Geophys. Res.* **97**(D9), 10 145–10 156.
- Plumb, R. A. and McConalogue, D. D. 1988. On the meridional structure of long-lived tropospheric constituents. *J. Geophys. Res.* **93**(D12), 15 897–15 913.
- Popp, B. N., Westley, M. B., Toyoda, S., Miwa, T., Dore, J. E. and co-authors 2002. Nitrogen and oxygen isotopomeric constraints on the origins and sea-to-air flux of N₂O in the oligotrophic subtropical North Pacific gyre. *Global Biogeochem. Cycles* **16**, doi:2001GB001806.

- Potter, C. S., Matson, P. A., Vitousek, P. M. and Davidson, E. A. 1996. Process modeling of controls on nitrogen trace gas emissions from soils worldwide. *J. Geophys. Res.* **101**(D1), 1361–1377.
- Prather, M., Ehhalt, D., Dentener, F., Derwent, R., Dlugokencky, E. and co-authors 2001. Atmospheric chemistry and greenhouse gases. In: *Climate Change 2001: the Scientific Basis. Contribution of Working Group I to the Third Assessment Report of the Intergovernmental Panel on Climate Change* (eds J. T. Houghton et al.). Cambridge University Press, Cambridge, 239–287.
- Prinn, R. G., Weiss, R. F., Fraser, P. J., Simmonds, P. G., Cunnold, D. M. and co-authors 2000. A history of chemically and radiatively important gases in air deduced from ALE/GAGE/AGAGE. *J. Geophys. Res.* **105**(D14), 17 751–17 792.
- Reynolds, R. W., Rayner, N. A., Smith, T. M., Stokes, D. C. and Wang, W. 2002. An improved in situ and satellite SST analysis for climate. *J. Climate* **15**(13), 1609–1625.
- Rintoul, S. and Trull, T. 2001. Seasonal evolution of the mixed layer in the Subantarctic Zone south of Australia. *J. Geophys. Res.* **106**(C12), 31 447–31 462.
- Seitzinger, S. P. and Kroeze, C. 1998. Global distribution of nitrous oxide production and N inputs in freshwater and coastal marine ecosystems. *Global Biogeochem. Cycles* **12**, 93–113.
- Stephens, B. B., Keeling, R. F., Heimann, M., Six, K. D., Murnane, R. and co-author 1998. Testing global ocean carbon cycle models using measurements of atmospheric O₂ and CO₂ concentration. *Global Biogeochem. Cycles* **12**, 213–230.
- Suntharalingam, P. and Sarmiento, J. L. 2000. Factors governing the oceanic nitrous oxide distribution: simulations with an ocean general circulation model. *Global Biogeochem. Cycles* **14**, 429–454.
- Takahashi, T., Poisson, A., Metzl, N., Tilbrook, B., Bates, N. and co-authors 2002. Global sea-air CO₂ flux based on climatological surface ocean pCO₂, and seasonal biological and temperature effects. *Deep-Sea Res. II* **49**, 1601–1622.
- Taylor, J. A. 1992. A global three-dimensional Lagrangian tracer transport modeling study of the sources and sinks of nitrous oxide. *Math. Comput. Simulat.* **33**, 597–602.
- Toyoda, S., Yoshida, N., Miwa, T., Matsui, Y., Yamagishi, H. and co-authors 2002. Production mechanism and global budget of N₂O inferred from its isotopomers in the western North Pacific. *Geophys. Res. Lett.* **29**(3), doi:10.1029/2001GL014311.
- Volk, C. M., Elkins, J. W., Fahey, D. W., Dutton, G. S., Gilligan, J. M. and co-authors 1997. Evaluation of source gas lifetimes from stratospheric observations. *J. Geophys. Res.* **102**(D21), 25 543–25 564.
- Wanninkhof, R. 1992. Relationship between wind speed and gas exchange over the ocean. *J. Geophys. Res. Oceans* **97**(C5), 7373–7382.
- Ward, B. B. 1986. Nitrification in marine environments. In: *Nitrification* (ed. J. I. Prosser), IRL Press, Washington, DC, 157–184.
- Weiss, R. F. 1981. The temporal and spatial distribution of tropospheric nitrous oxide. *J. Geophys. Res.* **86**, 7185–7195.
- Weiss, R. F. and Price, B. A. 1980. Nitrous oxide solubility in water and seawater. *Mar. Chem.* **8**, 347–359.
- Yoshinari, T. 1976. Nitrous oxide in the sea. *Mar. Chem.* **4**, 189–202.